



A Heterodyne Interferometer with Separated Beam Paths for High-Precision Displacement and Angular Measurements

Guido Straube¹ · Juan Sebastian Fischer Calderón¹ · Ingo Ortlepp¹ · Roland Füßl¹ · Eberhard Manske¹

Received: 31 December 2020 / Revised: 15 February 2021 / Accepted: 25 February 2021 / Published online: 23 April 2021
© The Author(s) 2021

Abstract

As standard concepts for precision positioning within a machine reach their limits with increasing measurement volumes, inverse concepts are a promising approach for addressing this problem. The inverse principle entails other limitations, as for high-precision positioning of a sensor head within a large measurement volume, three four-beam interferometers are required in order to measure all necessary translations and rotations of the sensor head and reconstruct the topography of the reference system consisting of fixed mirrors in the x -, y -, and z -directions. We present the principle of a passive heterodyne laser interferometer with consequently separated beam paths for the individual heterodyne frequencies. The beam path design is illustrated and described, as well as the design of the signal-processing and evaluation algorithm, which is implemented using a System-On-a-Chip with an integrated FPGA, CPU, and A/D converters. A streamlined bench-top optical assembly was set up and measurements were carried out to investigate the remaining non-linearities. Additionally, reference measurements with a commercial homodyne interferometer were executed.

Keywords Heterodyne laser interferometer · He–Ne laser · Optical fiber coupling · Beat frequency · Non-linearities

1 Introduction

Recent developments in semiconductor production technologies, namely the increased diameter of processed wafers and the simultaneous diminishment of structure pitches, lead to challenging requirements with regard to production as well as the measurement of the produced structures. Therefore, the demand for high dynamic measurements with high precision in large measurement volumes is growing. In order to address these tasks, nano positioning and nano measuring machines (NPMs) were developed. Figure 1 depicts the basic layout of two prominent representatives of this category, the NMM1 and NPMM-200, developed at the Technische Universität Ilmenau [1, 2]. The NPMM-200 has a measurement volume of $200 \times 200 \times 25 \text{ mm}^3$, whereas the movement is realized by a stage on which the measured object is located. The displacement measurement is realized with fiber-coupled laser interferometers, typically used for accurate non-contact, traceable length measurements with

high dynamic demands and resolutions in the sub-nanometer range [3]. Three interferometers, one for every spatial axis, are mounted to a fixed metrological frame. The virtual point of intersection of the individual homodyne interferometer beams is located in the contact point of the fixed probe and the measurement object, hence the Abbe principle is followed consequently, which allows for nanoscale accuracy by the elimination of first-order measurement errors.

With the mentioned increasing demands on the size of the measuring volume, this principle reaches its limits as the size of the stage needs to be scaled up with a growing measuring volume, which consecutively leads to an increase of the mass to be moved. This stands in contrast to the high dynamic demands on the movement of the stage, as with increasing measurement volume and constant measuring time, the velocity and acceleration of the stage need to be increased. In order to evade this undesired development, a new inverse concept for an NPM is proposed in [4]. The core element of this new concept is a moving measuring head to which the interferometers and the probe are attached. The reference system consists of fixed mirrors in x -, y - and z -directions. With the measurement object also being fixed, all heavy elements are at rest. Therefore, the mass to be moved for a comparable measurement volume

✉ Guido Straube
guido.straube@tu-ilmenau.de

¹ Technische Universität Ilmenau, Ehrenbergstraße 29,
98693 Ilmenau, Germany

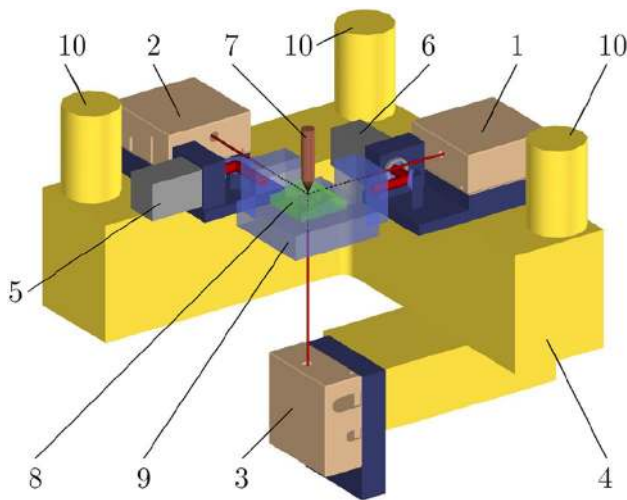


Fig. 1 Basic layout of the NMM1 and NPMM-200: 1 *x*-interferometer, 2 *y*-interferometer, 3 *z*-interferometer, 4 Zerodur frame, 5 roll and yaw angle sensor, 6 pitch and yaw angle sensor, 7 probe system, 8 measuring object, 9 mirror corner, 10 mounting points for probe system [1]

is significantly smaller when using the inverse concept than when utilizing the classic one. In order to control the position and orientation of the sensor head when moving through the measuring volume, in theory two interferometer axes per movement direction are sufficient. However, as the fixed mirrors are not perfectly flat, especially when considering large dimensions up to an axis length of 1 m, this poses a new challenge, as the reconstruction of the mirrors topographies is of essential importance for the achievable precision. Determining the mirrors' topographies with an external calibration is not practical, as the shape would change significantly when mounting the mirrors to the machine frame. Thus, an *in situ* calibration of the measurement mirrors is advisable. This can be done with data obtained from two length-measurement systems, which need to be arranged one behind the other in direction of the movement [5, 6]. Therefore, in every spatial axis, three interferometer beams are necessary.

In order to measure displacement as well as angular deviations, the use of several individual interferometers is conceivable. However, for the above-described application with limited installation space and, in order to fulfill the high dynamic demands on the movement of the measuring head, a weight as low as possible, a single interferometer with multiple measuring beams is a more convenient solution.

2 State of the Art

Heterodyne laser interferometers (HIFs) rely on periodic alternating phase signals in order to obtain length values. The phase of a measuring beam is evaluated against a reference beam, hence amplitude and offset of the signals are of minor importance. For this reason, HIFs are typically utilized for applications where multiple measuring beams need to emerge from one interferometer head because the requirements for the intensity of a single beam are significantly lower than the case of a homodyne interferometer. Furthermore, the concept allows for straightforward implementation of multiple beams when designing the optical beam path.

Extensive research on HIFs has been carried out and published, whereas HIFs are utilized for displacement measurements by Lawall et al. [7], Gillmer et al. [8], Yan et al. [9], and Yu et al. [10]. Other publications, such as Shi et al. [11] or Jin et al. [12], use heterodyne multi-beam interferometers for straightness and roll angle measurements. All the mentioned publications, except for Jin et al., use optical setups based on the classic Michelson interferometer design. HIFs based on this design typically provide the ability to compensate for source intensity changes, but are prone to systematic periodic errors because of the possibility of mixing of the different frequencies [13], as well as ghost reflections and deviations in the evaluation electronics [14]. These effects are analyzed in depth by Wu et al. [15] and Xing et al. [16].

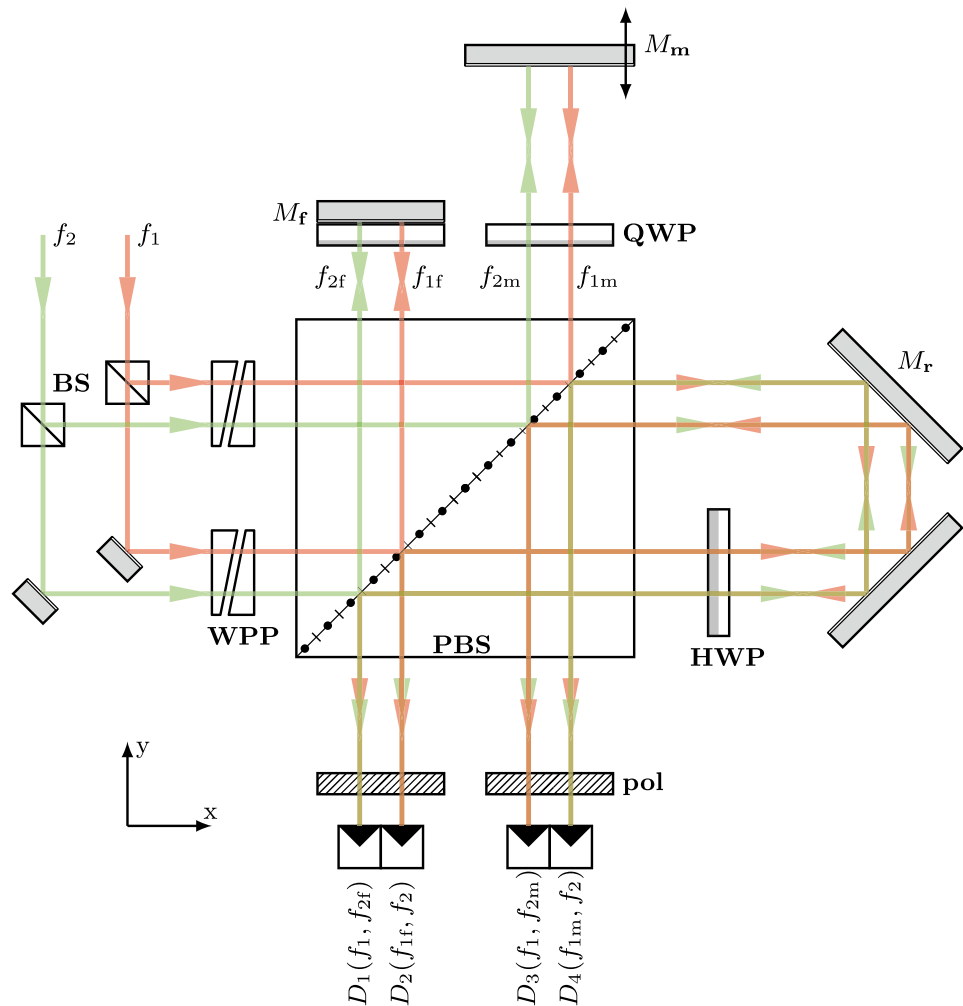
The main difference between the above-mentioned HIF setups and the novel one proposed here, is the number and arrangement of the measuring beams and their spatial separation. Additionally, the two laser frequencies are not realized by acousto-optic modulators but by two phase locked He–Ne lasers [17]. The described inverse concept for NPMs relies on at least three measuring beams in one spatial axis, but, for symmetry reasons, four measuring beams instead of the required three are implemented in the concept. A measuring head in an NPMM with an inverse concept would hence consist of three modules of the proposed HIF; one for the *x*-, one for the *y*- and one for the *z*-direction. The effect of frequency mixing related non-linearities is minimized by consequent spatial separation of the individual beam paths. The remaining non-linearities are analyzed and discussed in Sect. 4.2.

3 Principle of Operation

3.1 Beam Path and Characteristics

Figure 2 represents a simplified beam path of the proposed HIF, designed to comply to the demands mentioned in Sects. 1 and 2. In order to achieve four measuring beams on

Fig. 2 Simplified beam path of the HIF. BS: non-polarizing beam splitters, WPP: wedge plate pairs, PBS: polarizing beam splitter, QWP: quarter wave plate, HWP: half wave plate, M_m : moving mirror, M_f : fixed mirror, M_r : reference mirror, pol: 45° polarizers, D_{1-4} : photodiodes



the measuring mirror while spatially separating the two frequencies, eight beams need to enter the PBS. Accordingly, the beam path is split into two levels, whereas Fig. 2 only displays one level. Therefore, the beam splitting assembly depicted on the left side is also simplified.

The two beams with the frequencies f_1 and f_2 emerge from He–Ne lasers which are beat frequency controlled by a phase-locked-loop. As the light with the frequencies f_1 and f_2 originates from individual He–Ne lasers and is delivered to the bench-top setup by separate polarization maintaining fibers, mutual influence is ruled out. Additionally, the beat frequency is tunable and experiments showed a beat frequency stability of $4.5 \cdot 10^{-5}$ [17]. The relation between the two frequencies is described in Eq. (1).

$$f_{\text{beat}} = f_1 - f_2 = 4 \text{ MHz} \quad (1)$$

After the beam splitting assembly, the incoming beams pass adjustable wedge plate pairs, which serve as compensation tools for deviations from the ideal geometry of the

preceding and following optical elements and ensure that all beams are parallel. When entering the PBS, the light is linearly polarized at 45°. The eight parallel beams pass through the PBS, where the s-polarized proportion of each beam is deflected towards the moving mirror M_m and the fixed mirror M_f . In this arm of the HIF, the polarization is altered by quarter-wave plates, through which the beams pass two times. Therefore, the reverting beams are p-polarized and pass straight through the splitting layer of the PBS.

The p-polarized proportion is guided through the PBS to the retroreflecting reference mirror M_r , where the beams pass a half wave plate. Therefore, the returning beams are deflected because of their s-polarization and united with the beams from M_m and M_f . The superimposed beams will not interfere, as their polarizations are in planes which are perpendicular to each other. After passing through the polarizers set to 45°, the superimposed beams interfere. The composition of the signals detected by the photodiodes D_{1-4} is shown in Fig. 2, whereas the indices of the frequencies correspond to the mirrors they are reflected by, except for the mirror M_r , as the beams passing through this arm serve as reference and are present on every

diode. This notation is used in Eqs. (2) and (3) too. Presuming M_m is fixed, the signals of both photodiodes D_1 and D_4 show the beat frequency. When M_m does move, the interference pattern on the photodiode D_1 still shows the beat frequency, while the pattern on D_4 represents the beat frequency overlaid with the Doppler frequency f_Δ , as shown in Eq. (2).

$$\begin{aligned}
 f_{1f} &= f_1 \\
 f_{2f} &= f_2 = f_1 - f_{\text{beat}} \\
 f_{1m} &= f_1 + f_\Delta \\
 f_{2m} &= f_2 + f_\Delta = f_1 - f_{\text{beat}} + f_\Delta
 \end{aligned}
 \tag{2}$$

Equation (3) displays the theoretical signals s_{beat} and s_{meas} detected by the photodiodes D_1 and D_4 . Since the frequencies f_1 and f_2 are known, the absolute value and sign of f_Δ can be determined by comparing s_{meas} and s_{beat} . Hence, the direction and velocity of the mirror, respectively of the measuring head in the proposed inverse concept, can be calculated. Equation (4) describes the relation of beat frequency and mirror velocity v_m . As an example, a numerical value for an assumed Doppler frequency of $f_\Delta = 0.3478$ MHz and the typical wavelength $\lambda_L = 632.8$ nm for a He–Ne laser is calculated in Eq. (4).

$$\begin{aligned}
 D_1 : s_{\text{beat}} &= f_1 - f_{2f} = f_1 - f_1 + f_{\text{beat}} \\
 D_4 : s_{\text{meas}} &= f_{1m} - f_2 = f_1 - f_1 + f_{\text{beat}} + f_\Delta
 \end{aligned}
 \tag{3}$$

$$v_m = \frac{1}{2} \cdot f_\Delta \cdot \lambda_L = 0.11 \frac{\text{m}}{\text{s}}
 \tag{4}$$

To avoid a zero-crossing when comparing the beat and Doppler frequencies, a maximum velocity and therefore, a maximum Doppler frequency needs to be chosen. With a beat frequency of 4 MHz, the maximum measurable velocity of the measuring mirror is $\approx 1.27 \frac{\text{m}}{\text{s}}$.

3.2 Signal Processing

In order to obtain the phase difference between s_{beat} and s_{meas} , the lock-in-principle is utilized. Therefore, the signals need to be mixed and filtered in order to shift them to the base band. Subsequently, the conventional homodyne arc tangent demodulation can be used. Figure 3 gives an overview of the signal processing sequence, which is implemented on a ‘‘Red Pitaya’’ [18], a System-On-a-Chip with an integrated FPGA, CPU, and two A/D converters. The clock frequency of the system is 125 MHz.

In Fig. 4a, the theoretical raw signals are shown; Fig. 4b depicts the Fourier transformation of the signals. These diagrams correspond to the position of marker (1) in Fig. 3. By multiplying the signals s_{beat} and s_{meas} with $f_{\text{LO}} \approx f_{\text{beat}}$, the signals are shifted to the base band. This corresponds to the position of marker (2) in Fig. 3. From this mathematical operation, unwanted mixing products outside the base band occur, as Eq. (5) shows. Here, the part $\cos(f_1 + f_2)$ describes the higher frequency, in Fig. 5c visualized as the second peak at approximately 8 MHz. This superimposed oscillation is suppressed by a low-pass filter, whose threshold frequency needs to be greater than the beat frequency. Hence, a value of 5 MHz is chosen.

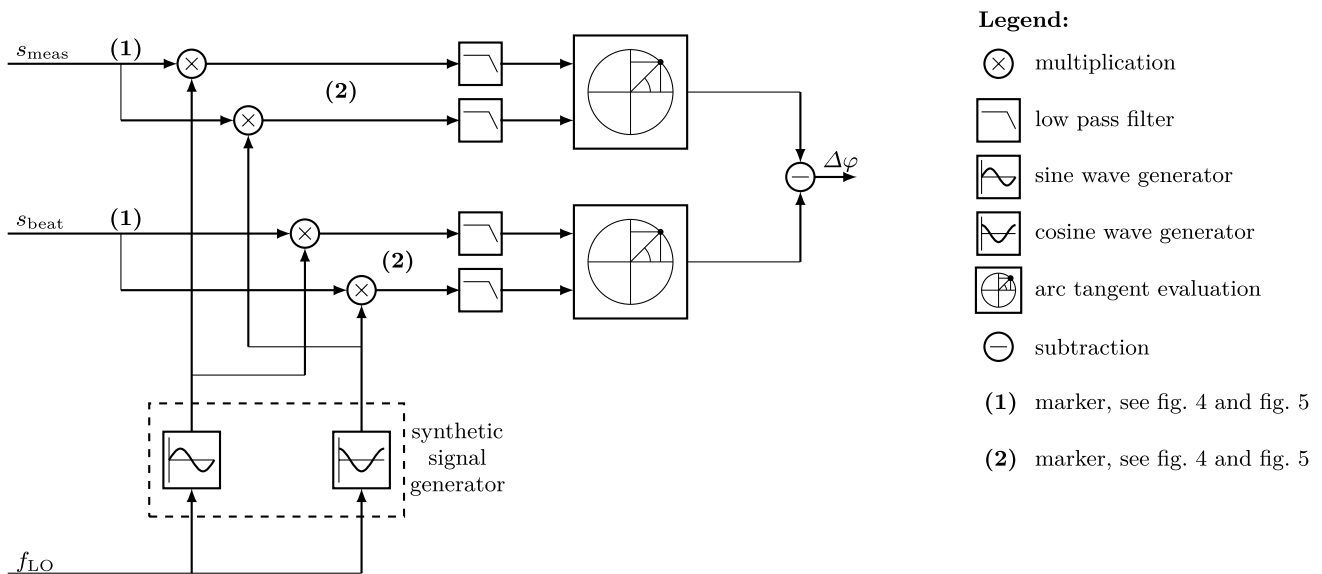
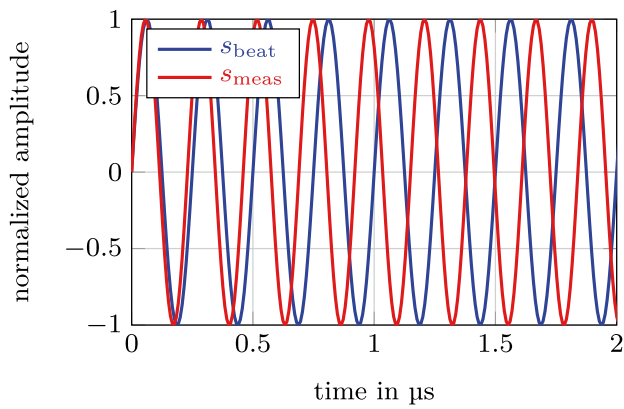
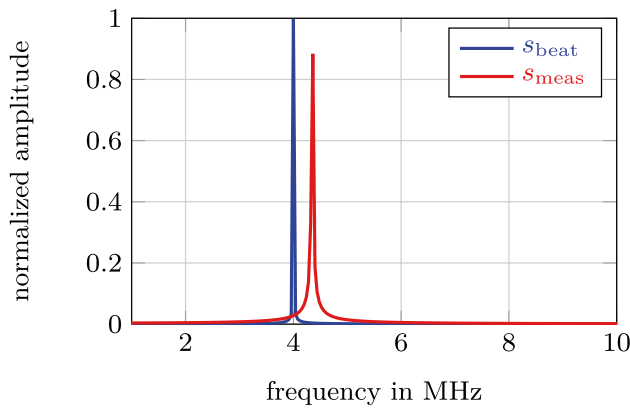


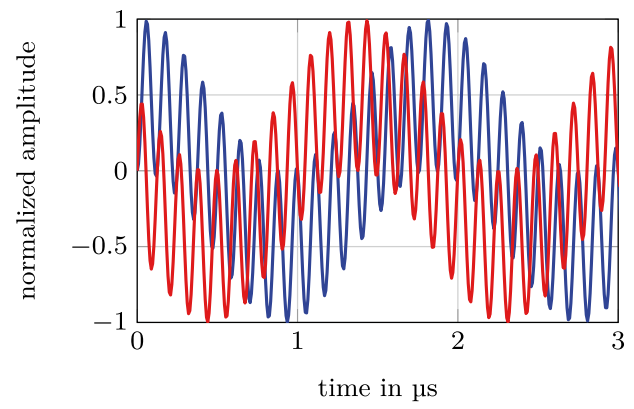
Fig. 3 Signal flow of the data acquisition platform, s_{meas} is the signal detected by D_4 , s_{beat} the signal detected by D_1 (see Fig. 2), $f_{\text{LO}} = 4$ MHz and $\Delta\phi$ the phase angle difference in between both signals



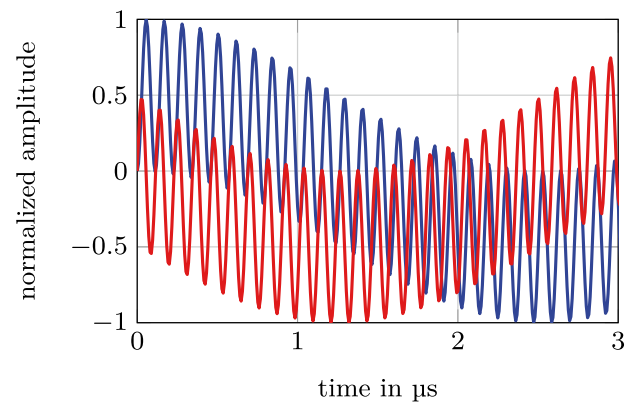
(a) theoretical raw signals



(b) Fourier transformed raw signals



(a) in blue: $s_{\text{beat}} \cdot \sin(4 \text{ MHz})$,
in red: $s_{\text{beat}} \cdot \cos(4 \text{ MHz})$



(b) in blue: $s_{\text{meas}} \cdot \sin(4 \text{ MHz})$,
in red: $s_{\text{meas}} \cdot \cos(4 \text{ MHz})$

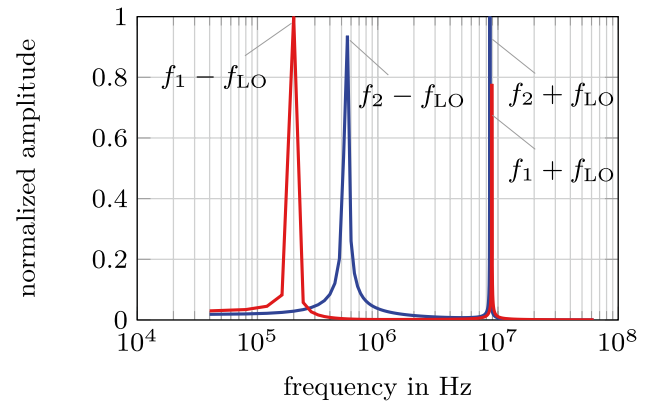
Fig. 4 Theoretical raw values; see position (1) in Fig. 3

$$\sin(f_1) \cdot \sin(f_2) = \frac{1}{2} (\cos(f_1 - f_2) - \cos(f_1 + f_2)) \quad (5)$$

$$\Delta\varphi = \varphi_{\text{meas}} - \varphi_{\text{beat}} \quad (6)$$

$$L = \frac{\Delta\varphi}{2\pi} \cdot \frac{\lambda}{2} \quad (7)$$

From these signals, the phase angle is calculated by the arc tangent. When subtracting these signals one from the other, the phase angle difference $\Delta\varphi$ and thus, the optical path difference between measurement and reference arm of the HIF is obtained. The result is depicted in Fig. 6. Caused by the layout of the beam path, the presented HIF has a sensitivity of $\frac{\lambda}{2}$. Hence, to obtain length values L , the operation denoted in Eq. (7) needs to be applied.



(c) in blue: $\mathcal{F}(s_{\text{beat}} \cdot \sin(4 \text{ MHz}))$,
in red: $\mathcal{F}(s_{\text{meas}} \cdot \sin(4 \text{ MHz}))$

Fig. 5 Theoretical values after mixing; see position (2) in Fig. 3

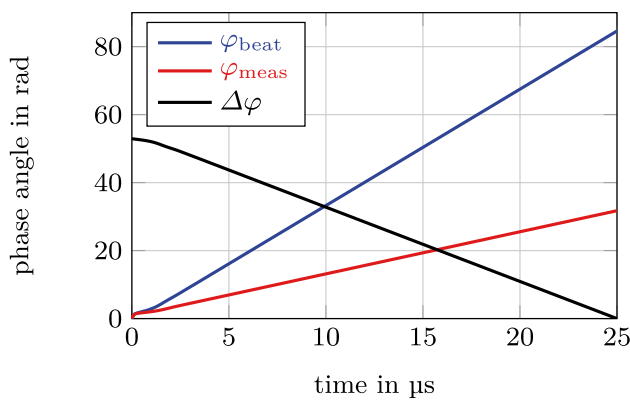


Fig. 6 Resulting phase angle with minimum shifted to zero

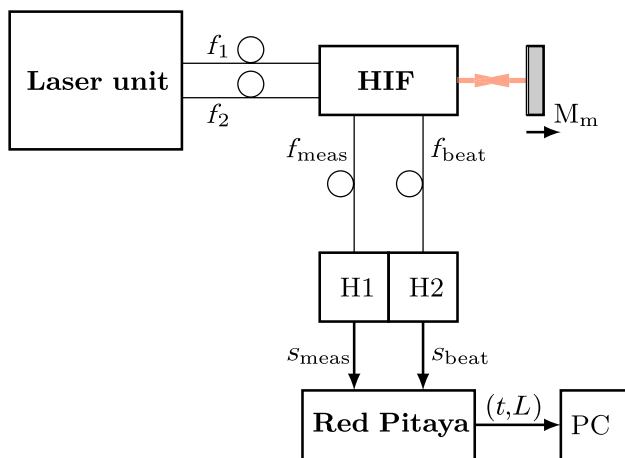


Fig. 7 Schematic representation of the setup: M_m : measuring mirror mounted to heatable brass rod, “H1” and “H2”: Hamamatsu C5658 avalanche photo diode modules [19], (t,L) : time stamps and length signals

4 Experimental Results

4.1 Setup

In order to determine the extent of the remaining non-linearities and environmental errors, a streamlined bench-top optical assembly of the proposed HIF is set up, as depicted in Fig. 7. In this minimal configuration, only one of the four beams on the measuring mirror is present. Hence, only the displacement of the mirror can be measured. To realize the movement of the mirror M_m , it is mounted to a heatable brass rod. Opposed to the representation in Fig. 2, after passing through the optical system, the superimposed beams are coupled into multi-mode optical fibers by lenses. On the output side, the fibers are connected to Hamamatsu C5658 avalanche photo diode modules [19]. The obtained analog signals are then passed to the “Red Pitaya” board where the signals are A/D converted and analyzed as described in Sect. 3.2. The phase angle

difference values $\Delta\varphi$, together with time stamps to ensure the evaluability, are then transmitted to a PC via Ethernet. The proposed full HIF setup, as well as the here-used streamlined bench-top version, are completely passive, as optical fibers are used to supply the heterodyne frequencies to the optical assembly and to return the interferometer signals to the evaluation unit. This holds an advantage, as there is no power dissipation inside the measuring head and therefore no heat and no electrical disturbance input into the measuring volume.

In order to generate comparative data, reference measurements with a commercial homodyne laser interferometer are carried out, utilizing the same heatable brass rod as mount for the measuring mirror.

4.2 Results

The heated rod is brought to temperature and the cooling process is measured one after the other with both measuring devices, the minimal bench-top setup of the proposed HIF and the commercial homodyne laser interferometer. None of the devices is vibrationally decoupled from the environment and the obtained data is not corrected for changes in the refractive index of the ambient air. Therefore, both measurement systems are biased by comparable environmental influences and thus, can be assumed to be in the same range. Furthermore, multiple measurements were carried out to ensure the peaks found in the Fourier transform are not caused by random environmental influences.

As the length change of the rod caused by a temperature change is proportional to the e-function, the named function is fitted to the obtained length data, as shown in Figs. 8a and 9a and subsequently subtracted. At this point, the non-linearities become visible as periodic deviations from an ideal straight line, as shown in Fig. 8b and 9b, whereas the red lines depict the data set filtered by a moving average filter with a window size of 500 values. To characterize the non-linearities, a Fourier transformation is applied to the unfiltered data set. The results are displayed in Figs. 8c and 9c.

The data obtained by the proposed HIF setup shows a peak at approx. $\frac{\lambda}{2}$ with an amplitude of 0.22 nm. The reference measurement shows no distinctive peak at $\frac{\lambda}{2}$, but one at approx. $\frac{\lambda}{4}$, with an amplitude of 0.35 nm and one at approx. $\frac{\lambda}{8}$, with an amplitude of 0.55 nm. Hence, the non-linearities observed with the HIF setup are significantly smaller than the ones observed with the commercial homodyne interferometer setup, namely by a factor of 2.5.

When comparing these results with the measurements published in [16], it becomes clear that there is potential for improvement, as the minimal periodic nonlinear error found with the setup proposed by Xing et al. can approach 0.086 nm.

As the frequency mixing inside the optical path of the HIF is minimized by design, the present non-linearities are caused

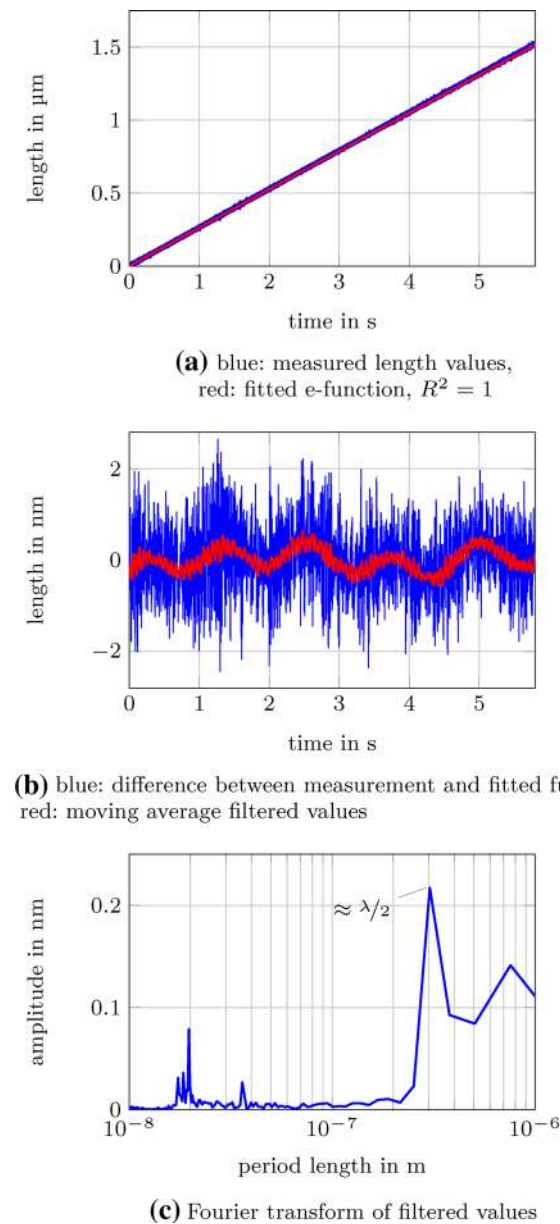


Fig. 8 Measurement results, recorded with minimal benchtop setup of the proposed HIF

by deviations in the signal processing and ghost reflections. Nevertheless, the error is lower by a factor of 2.5 than the one present in the reference measurements, which testifies to a great potential of the proposed HIF.

5 Conclusions and Outlook

A heterodyne interferometer concept with four interferometric axes has been investigated. As a functional verification, a streamlined bench-top version was set up and an algorithm for data acquisition and evaluation

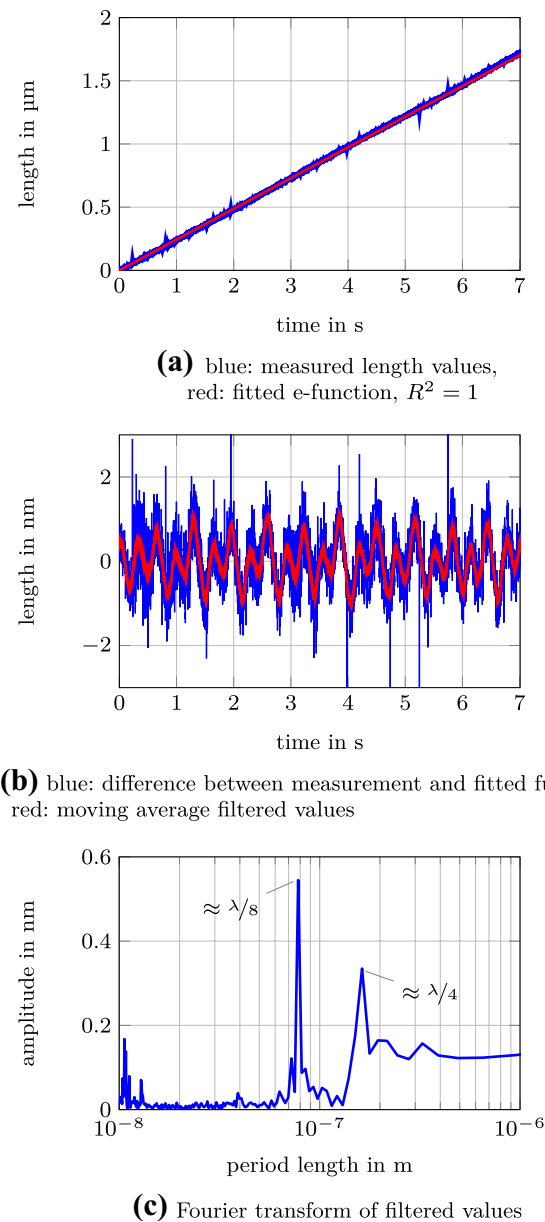


Fig. 9 Reference measurement results, recorded with commercial homodyne laser interferometer

was developed. This algorithm allows compensating for changes in the laser source intensity and for changes of the beat frequency. The optical design of the HIF focuses on the minimization of periodic non-linearities by consequent spatial separation of the beam paths of the individual heterodyne frequencies. Additionally, in order to avoid heat dissipation into the measuring volume, the optical assembly of the interferometer is fiber-coupled and therefore completely passive. Measurements were carried out to determine the characteristics of the HIF concept regarding non-linearities. It is shown that these non-linearities are smaller than 0.22 nm at $\frac{\lambda}{2}$. Additionally,

reference measurements were performed with a commercial homodyne interferometer, which shows significantly higher amplitudes at $\frac{\lambda}{4}$ and $\frac{\lambda}{8}$. Nevertheless, attention will be paid to further decrease the amount of the deviations present in the measurements carried out with the HIF by optimizing the optical layout as well as the electronic phase evaluation.

In the next step, the setup will be expanded to all four measuring beams, which will allow for angular measurements. The results of these measurements will be compared to high-accuracy autocollimators and commercial two beam laser interferometers. Additional measurements include the determination of drift characteristics and the resolution limit, as well as the performance over large distance ranges and the reconstruction of sampled mirror topographies with the method proposed in [5].

The further development, also in regard to the proposed inverse concept for NPMMs, includes a miniaturized HIF module. As three modules need to be attached to the moving sensor head, the focus will lie on lightweight and compact design as well as on simple and convenient adjustability.

Acknowledgements This project was funded by the Deutsche Forschungsgemeinschaft (DFG) under contract 279458870.

Funding Open Access funding enabled and organized by Projekt DEAL.

Data Availability Data and material are available upon request.

Code Availability Code is available upon request.

Declarations

Conflict of interest The authors declare that they have no conflict of interest.

Open Access This article is licensed under a Creative Commons Attribution 4.0 International License, which permits use, sharing, adaptation, distribution and reproduction in any medium or format, as long as you give appropriate credit to the original author(s) and the source, provide a link to the Creative Commons licence, and indicate if changes were made. The images or other third party material in this article are included in the article's Creative Commons licence, unless indicated otherwise in a credit line to the material. If material is not included in the article's Creative Commons licence and your intended use is not permitted by statutory regulation or exceeds the permitted use, you will need to obtain permission directly from the copyright holder. To view a copy of this licence, visit <http://creativecommons.org/licenses/by/4.0/>.

References

- Hausotte T (2002) Nanopositionier- und Nanomeßmaschine. Dissertation, TU Ilmenau
- Jäger G, Manske E, Hausotte T, Müller A, Balzer F (2016) Nanopositioning and Nanomeasuring Machine NPMM-200 - a new powerful tool for large-range micro- and nanotechnology. *Surf. Topogr. Metrol. Prop.* 4:034004. <https://doi.org/10.1088/2051-672X/4/3/034004>
- Manske E, Fröhlich T, Füssl R, Mastlyo R, Blumröder U, Köchert P, Birli O, Ortlepp I, Pruss C, Schwesinger F, Meister A (2019) Scale spanning subnanometer metrology up to ten decades. In: *Proceedings volume 11056, optical measurement systems for industrial inspection XI*, 110560L. <https://doi.org/10.1117/12.2526076>
- Straube G, Fischer Calderón SJ, Ortlepp I, Manske E (2020) Fundamentals of dynamic sensor positioning with nanoscale accuracy by an inverse kinematic concept. *SMSI 2020—Measurement Science, D6 Inverse Problems in Measuring Technology*. <https://doi.org/10.5162/SMSI2020/D6.4>
- Schulz M, Elster C (2006) Traceable multiple sensor system for measuring curved surface profiles with high accuracy and high lateral resolution. *Opt Eng* 45(6):060503. <https://doi.org/10.1117/1.2208568>
- Wiegmann A, Schulz M, Elster C (2010) Improving the lateral resolution of a multisensor profile measurement method by non-equidistant sensor spacing. *Opt Soc Am Opt Express*. <https://doi.org/10.1364/OE.18.015807>
- Lawall J, Kessler E (2000) Michelson interferometry with 10 pm accuracy. *Rev Sci Instrum* 71:2669. <https://doi.org/10.1063/1.1150715>
- Gillmer SR, Smith RCG, Woody SC, Ellis JD (2014) Compact fiber-coupled three degree-of-freedom displacement interferometry for nanopositioning stage calibration. *Meas Sci Technol* 25:075205. <https://doi.org/10.1088/0957-0233/25/7/075205>
- Yan H, Duan H-Z, Li L-T, Liang Y-R, Luo J, Yeh H-C (2015) A dual-heterodyne laser interferometer for simultaneous measurement of linear and angular displacements. *Rev Sci Instrum* 86:123102. <https://doi.org/10.1063/1.4936771>
- Yu X, Gillmer SR, Woody SC, Ellis JD (2016) Development of a compact, fiber-coupled, six degree-of-freedom measurement system for precision linear stage metrology. *Rev Sci Instrum* 87:065109. <https://doi.org/10.1063/1.4953335>
- Shi K, Su J, Hou W (2018) Roll angle measurement system based on differential plane mirror interferometer. *Opt Soc Am Opt Express*. <https://doi.org/10.1364/OE.26.019826>
- Jin T, Han M, Liu J, Le Y, Hou W (2019) A heterodyne interferometer for simultaneous measurement of roll and straightness. *IEEE Access*. <https://doi.org/10.1109/ACCESS.2019.2941078>
- Dannberg O, Ortlepp I, Manske E (2017) FPGA-based signal processing of a heterodyne interferometer. *Ilmenau Scientific Colloquium. Technische Universität Ilmenau*; 59 (Ilmenau): 2017.09.11-15
- Weichert C, Köchert P, Köning R, Flügge J, Andreas B, Kuetgens U, Yacoot A (2012) A heterodyne interferometer with periodic nonlinearities smaller than ± 10 pm. *Meas Sci Technol* 23:094005. <https://doi.org/10.1088/0957-0233/23/9/094005> (7)
- Wu C-M, Lawall J, Deslattes RD (1999) Heterodyne interferometer with subatomic periodic nonlinearity. *Opt Soc Am Appl Opt*. <https://doi.org/10.1364/AO.38.004089>
- Xing X, Chang D, Hu P, Tan J (2017) Spatially separated heterodyne grating interferometer for eliminating periodic nonlinear errors. *Opt Soc Am Opt Express* 31384:31384. <https://doi.org/10.1364/OE.25.031384>
- Sternkopf C, Diethold C, Gerhardt U, Wurmus J, Manske E (2012) Heterodyne interferometer laser source with a pair of two phase locked loop coupled He-Ne lasers by 632.8 nm. *Meas Sci Technol*. <https://doi.org/10.1088/0957-0233/23/7/074006>
- Red Pitaya, Red Pitaya Book. <https://redpitaya.com/media/uploads/Red-Pitaya-Book-februar-2019.pdf>. Accessed 19 Nov 2020
- Hamamatsu, APD module C5658. <https://hamamatsu.com/eu/en/product/type/C5658/index.html>. Accessed 3 Dec 2020